Empirical evaluation of attractive van der Waals potentials for type-purified single-walled carbon nanotubes

Erik K. Hobbie, Thomas Ihle, John M. Harris, and Matthew R. Semler

Department of Physics, Department of Coatings and Polymeric Materials, North Dakota State University, Fargo, North Dakota 58108, USA

(Received 13 March 2012; revised manuscript received 11 May 2012; published 22 June 2012)

van der Waals forces play a critical role in the structure and stability of single-wall carbon nanotube (SWCNT) materials. Thin films assembled from SWCNTs purified by electronic type show particular promise for flexible electronics applications, but mechanical durability remains an unresolved issue. Using transition resonances determined from spectroscopic measurements of type-purified SWCNTs deposited on quartz, coupled with analogous spectroscopic characterization of polydimethylsiloxane (PDMS) substrates, we use the Lifshitz theory of van der Waals dispersion interactions developed by Rajter and co-workers [Rajter *et al.*, Phys. Rev. B **76**, 045417 (2007)] to examine the influence of electronic type on van der Waals contact potentials in polymer-supported nanotube networks. Our results suggest a significantly stronger nanotube-nanotube and nanotube-polymer attraction for the semiconducting SWCNT fractions, consistent with recent measurements of the electronic durability of flexible transparent SWCNT coatings.

DOI: 10.1103/PhysRevB.85.245439 PACS number(s): 61.48.De, 78.67.Ch, 82.35.Np, 78.20.Bh

I. INTRODUCTION

van der Waals (vdW) forces play a significant role in the structural stability of matter across a broad range of chemistry, physics, and biology.[1–6] They also play a particularly important role in nanotechnology, where they dominate the short-range attraction between nanoparticles and can hinder their dispersion and manipulation.[7–11] For particles lacking a permanent dipole moment, vdW dispersion forces arise solely from small fluctuations in the electromagnetic field—or more precisely, the dielectric permittivity—across the space between the particles,[12,13] which is dominated by the zero-point energy of quantum vacuum fluctuations. The quantum-field nature of such a mundane, ubiquitous, and sometimes macroscopic force is quite remarkable, if on occasion not fully appreciated.

Single-wall carbon nanotubes (SWCNTs) are nanometer-thick tubes of graphene 100 nm to 100 μm in length. They can be either metallic or semiconducting, depending on the chiral vector (n,m) that characterizes the symmetry of rolling a two-dimensional (2D) graphene sheet into a hollow tube.[14] They are one of the most studied materials within the realm of modern nanotechnology, with exceptional physical properties that herald the possibility of significant technological potential.[15] The importance of vdW forces in SWCNT materials cannot be overstated. The high aspect ratio and strong anisotropy create potential wells thousands of k_BT in depth, but SWCNTs have yet to realize their full potential as mechanical reinforcing agents. This is primarily due to the mechanical failure of interfacial contacts, which are largely governed by vdW forces. Although chemical cross-linking can help mitigate such effects, this often occurs at the expense of the intrinsic SWCNT properties of interest,[16] which can limit the potential impact of applications.

Raw nanotube materials typically contain a broad distribution of lengths and a mixture of the two distinct electronic species, usually 1/3 metallic and 2/3 semiconducting. Recent advances in the separation of SWCNTs by length and electronic type, however, have ushered in a new era of research focused on the physical attributes and potential applications of highly monodisperse nanotube materials.[17–22] In particular, such purified SWCNTs show tremendous promise for flexible electronics applications,[23] where the mechanics of vdW contact forces will play a potentially profound role in dictating device durability and performance.[24,25] One recent study, for example, offered compelling evidence that electronic type can have a significant influence on the durability of flexible transparent SWCNT films, with metallic nanotubes offering improved performance over semiconducting nanotubes.[26]

The Lifshitz framework of vdW interactions has recently been cast in a form that can be readily applied to SWCNTs.[27] Building on the extensive work of French[28] and Parsegian,[29] Rajter *et al.*[27] have developed a formalism that offers considerable insight into the nature of vdW interactions in nanotubes. The scope of the work presented in Ref. 27 is ambitious in that it employs a first-principles *ab initio* scheme to compute the band structure of distinct chiral species. There are, however, some subtle but important issues that are not fully resolved by a purely theoretical approach. These include a dramatic depolarization effect that favors polarizations parallel to the nanotube axis,[30] the rather large influence of excitonic effects in quasi-1D systems,[31] and the overall challenge of accurately describing experimentally observed absorption spectra with an *ab initio* scheme. As an alternative, the approach we adopt here therefore relies on spectral data as a way to correctly, if only empirically, overcome these issues. By exploiting recent advances in the Lifshitz theory of vdW interactions applied to nanotubes, our goal is thus to address the role of SWCNT electronic type in dictating the magnitude of vdW contact forces, both between nanotubes and between nanotubes and a polymer substrate. Our results suggest a significantly stronger nanotube-nanotube and nanotube-polymer attraction for semiconducting SWCNTs on polydimethylsiloxane (PDMS), and we discuss these findings in the context of the electronic durability of flexible SWCNT coatings.[26]

II. MATERIALS AND METHODS

A rigorous implementation of the Lifshitz formalism requires a detailed knowledge of the imaginary part of the dielectric response function, $\epsilon(E) = \epsilon'(E) + i\epsilon''(E)$, over a

broad spectral range. For SWCNTs, this window (0–30 eV) naturally splits up into the three distinct regimes defined by Rajter and French.[32] These are delineated as "Drude" (0–0.1 eV), "π" (0.1–10 eV), and "σ" (> 10 eV). In the "Drude" regime, the response varies from metallic to semimetallic to semiconducting, depending on chirality. The "π" regime encompasses the familiar interband optical resonances up to the π plasmon and is typically accessed with UV-vis-NIR spectroscopy. The "σ" regime is dominated by the $\sigma + \pi$ plasmon and is correspondingly probed with electron energy loss spectroscopy (EELS).[32] This last regime dominates the spectral weight contained in the f-sum rule[33] and makes an appreciable contribution to the London dispersion spectra. Transitions associated with the σ/π electronic states emerge in the 12–20 eV range.[34–38]

Since we are interested in a generic chiral mixture of specific electronic types, our approach is to model the Drude regime with type-specific dielectric spectroscopy data and the π regime with type-specific UV-vis-NIR spectroscopy data. While the anisotropy and type dependence of the π plasmon are experimentally accessible, less is known about the $\sigma + \pi$ plasmon. Here, the resonant energy and relative strength of the oscillator are taken from EELS spectra of mixed-type SWCNTs, while the anisotropy and type dependence are assumed to follow the behavior exhibited by the π plasmon. This is a reasonable assumption, since both plasmons are graphitic features that acquire anisotropy through the tubular geometry. As a consistency check, we use the f-sum rule to ensure that the implied electron density is consistent with the range of diameters measured for each electronic type.

Details of the materials, purification scheme, and characterization methods—as well as the empirical scheme used to extract the intrinsic optical response from the data—can be found in the supporting information.[39] As shown in Fig. 1, a consequence of type purification is distinctly colored SWCNT fractions, blue for metallic and yellow/brown for semiconducting. In contrast, the polydimethylsiloxane (PDMS) substrates are colorless and transparent. As imaged in reciprocal space with small-angle light scattering [SALS, Fig. 1(c)] and in real space with transmission electron microscopy [TEM, inset Fig. 1(c)], the 10–100-nm-thick SWCNT membranes are isotropic and mesoporous networks of nanotube bundles with a mass-fractal dimension of 1.7. The colors of the components are evident in the absorption spectra, which we present in Fig. 2(a) as the imaginary part of the dielectric response function, $\epsilon''(E)$. As shown schematically in Fig. 2(b), there are three optical nanotube resonances for the semiconducting SWCNTs (denoted *11*, *22*, and *33*) but only one or two for the metallics (denoted *11* and *22*), where these correspond to

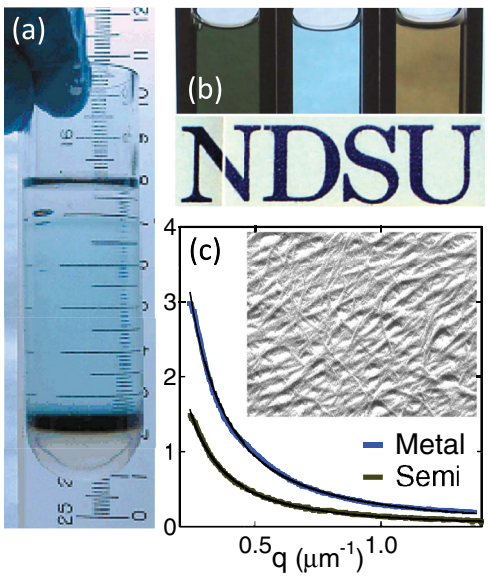

FIG. 1. (Color online) (a) Separation scheme, where the solvent density increases from top to bottom. The metallic SWCNTs move up and the semiconducting SWCNTs move down with respect to a layer of starting material at the blue-brown (light-dark) interface. (b) Colors of SWCNT solutions (top) before separation (left) and the metalic (middle) and semiconducting (right) fractions, with transparent PDMS (bottom). (c) SALS profiles from metallic and semiconducting films with a TEM image (inset) of the network morphology (scale = 250 nm) The curves are fits to the expression $I(q) \propto q^{-D}$ with $D = 1.72$. The scattering intensity has been reduced by the film thickness measured with atomic force microscopy (AFM) and the higher scattering in the metallic film is due to the near-resonant laser line.

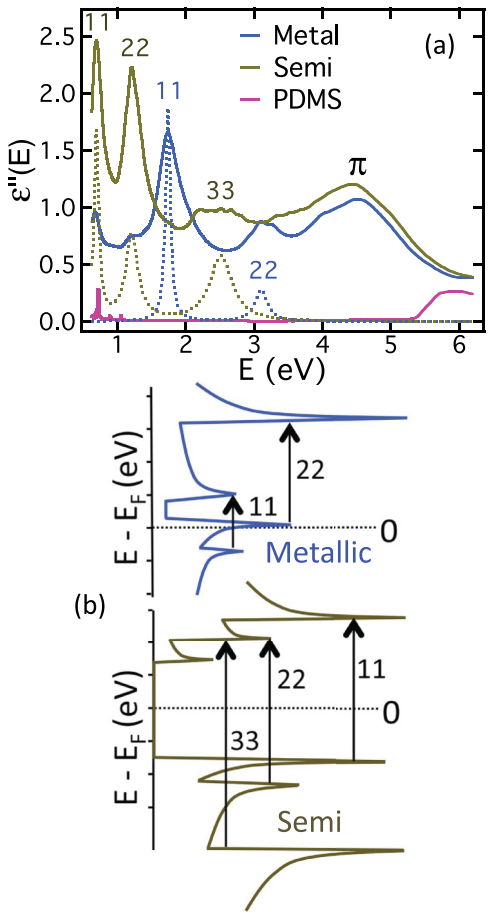

FIG. 2. (Color online) (a) Imaginary part of the dielectric response for the nanotubes and the polymer substrate with (b) a schematic of the SWCNT density of states near the Fermi energy for each type. The individual resonances deduced from the spectra (dashed) are reduced by a factor of 4 and the PDMS spectrum is amplified by a factor of 10^3 for clarity.

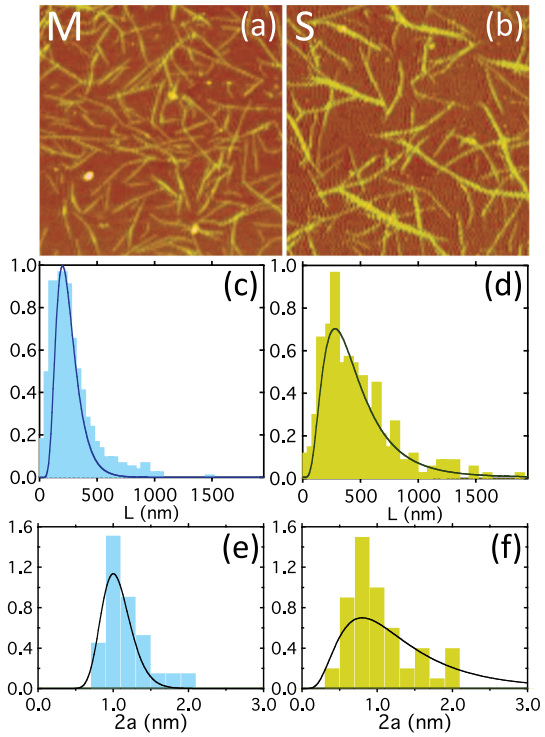

FIG. 3. (Color online) Force-microscopy images of (a) metallic and (b) semiconducting material on silicon, where each image is 2.4 μm tall. Samples were made by diluting 1% sodium deoxycholate SWCNT solutions of each electronic type 5:1 with purified water, and then soaking a piece of silicon wafer in each solution for 24 h. The samples were then soaked in ethanol for 3 h to remove surfactant. Length distributions are of isolated (c) metallic and (d) semiconducting SWCNTs, and diameter distributions are of isolated (e) metallic and (f) semiconducting SWCNTs.

interband transitions across the Fermi level.[31] As noted above, the anisotropy of the resonant features is well quantified, with the SWCNT transitions only occurring for polarizations along the nanotube axis and a slight anisotropy in the π plasmon due to the tubular geometry.[30,40] The transparent PDMS absorbs only in the NIR and UV [Fig. 2(a)].

As shown in Fig. 3, the type-purified solutions contain a broad distribution of lengths, ranging from 100 nm to 2 μm, with mean lengths of 300 and 475 nm for the metallic and semiconducting nanotubes, respectively. The diameter distribution is also broad, with a slightly smaller mean diameter for the semiconducting nanotubes ($\times$0.85). This diameter difference is further confirmed by radial-breathing-mode Raman spectroscopy (Fig. 4). A higher average density for the semiconducting SWCNTs would appear to be qualitatively consistent with the ultracentrifugation scheme [Fig. 1(a)] used to purify the nanotubes by electronic type,[26,39] but in reality the separation arises from small variations in the effective density of a solvated nanotube complex in a mixed-surfactant environment.[42] This diameter difference has significant implications for the problem of interest here, since the effective electron density of an equivalent tubular volume scales as $a/a^2 \sim 1/a$, which provides a constraint on the ratio of the f-sum rule applied to each ensemble.

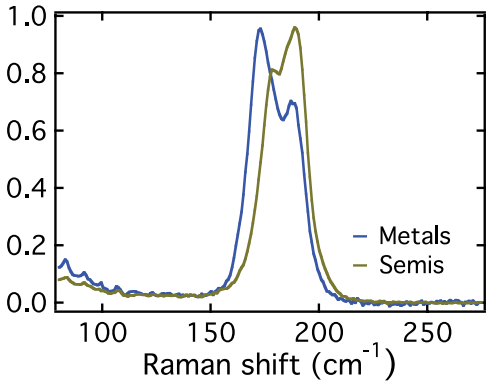

FIG. 4. (Color online) Radial breathing mode Raman spectra of the films on quartz depicted in Fig. 2. The average diameter of each ensemble scales inversely with the peak position, consistent with a smaller mean diameter for the semiconducting SWCNTs.

Although each SWCNT resonance in Fig. 2(a) represents a broad range of type-specific chiralities, we deduce the mean line shape by fitting the collective peak to a superposition of individual Lorentzians. Our only assumption is that the linewidth of the single-chiral response is the same for identical orders of resonance,[41] and as a point of reference we use the measured dielectric response of the (6, 5) SWCNT.[30] A realistic computational prediction of absolute oscillator strengths does not exist, so an empirical approach is the only viable option. Note that the location and strength of the individual resonances are critical in determining the London dispersion spectra, while the localized nature of the absorption features simplifies the analysis and interpretation. The measured spectra are also from bundled material, which underestimates the oscillator strengths of isolated SWCNTs in air. To correct for this, we use the ratio of the resonant extinction coefficients measured below (soluble) and above (aggregated) the intrinsic solubility limit for comparable metallic and semiconducting SWCNTs in alkyl-amide solvents.[39,43]

We are specifically interested in intimate nanotube contact, which is most relevant from the perspective of transparent conductive coatings. In the near-field limit within the Derjaguin approximation,[27] the nonretarded contact potential for two SWCNTs of identical type and diameter $2a$ depends on surface separation, ℓ, and orientation angle, θ, as

$$U(\ell,\theta) = -\frac{a(A_0 + A_2\cos^2\theta)}{6\ell\sin\theta}. \quad (1)$$

With air as the intervening medium, the Hamaker coefficients A_0 and A_2 are obtained as a Matsubara sum over all quantum modes, n, of the angular overlap in

$$\Delta\tilde{\epsilon} = \tilde{\epsilon}(i\xi_n) - 1, \quad (2)$$

where $\tilde{\epsilon}(i\xi_n)$ is the geometric mean of the in- and out-of-plane projections of the real part of the single SWCNT dielectric tensor,

$$\epsilon'_{ij}(\omega) = \delta_{ij} + \frac{2}{\pi}\int_0^\infty \frac{s\epsilon''_{ij}(s)}{s^2-\omega^2}ds, \quad (3)$$

evaluated at the imaginary frequencies

$$\xi_n = \frac{2\pi n k_B T}{\hbar}. \quad (4)$$

Explicitly, the Hamaker coefficients are

$$A_0 = \frac{3}{2} k_B T \sum_{n'} \left\langle \frac{\Delta\tilde{\epsilon}}{(\tilde{\epsilon}+1)} \frac{\Delta\tilde{\epsilon}_c}{(\tilde{\epsilon}_c+1)} \right\rangle \tag{5}$$

and

$$A_0 + A_2 = \frac{3}{2} k_B T \sum_{n'} \left\langle \frac{\Delta\tilde{\epsilon}^2}{(\tilde{\epsilon}+1)^2} \right\rangle, \tag{6}$$

where the prime in the sums denotes the usual Matsubara convention with the $n = 0$ term weighted by $1/2$. The brackets in Eqs. (5) and (6) denote an angular average over 2π in a variable ϕ that accounts for all possible directions within the plane normal to the direction of minimal surface separation ℓ. The subscript c denotes the substitution $\phi \to \pi/2 - \phi$ and

$$\tilde{\epsilon} = \sqrt{\epsilon_\perp(\epsilon_\perp \sin^2\phi + \epsilon_\parallel \cos^2\phi)}, \tag{7}$$

where $\epsilon_\perp$ and $\epsilon_\parallel$ denote the real part of the intrinsic SWCNT permittivities normal to and along the nanotube symmetry axis, respectively.[44] The two nanotubes cannot be parallel in our analysis and the assumption of close proximity implies infinite length.

Similarly, the near-field potential between a SWCNT of specific electronic type and an optically isotropic substrate follows from the cylinder-planar substrate interaction derived by Rajter *et al.* in the limit that the substrate is optically isotropic or non-birefringent.[27] The relevant expression for the potential is

$$U(\ell) = -\frac{\sqrt{2}}{24} \frac{L}{a} \left(\frac{a}{\ell}\right)^{3/2} A_0, \tag{8}$$

where the single Hamaker coefficient A_0 is obtained in an analogous fashion in terms of the substrate dielectric function ϵ_p as

$$A_0 = \frac{3}{2} k_B T \sum_{n'} \frac{\Delta\epsilon_p}{(\epsilon_p+1)} \left\langle \frac{\Delta\tilde{\epsilon}}{(\tilde{\epsilon}+1)} \right\rangle, \tag{9}$$

where $\Delta\epsilon_p = \epsilon_p - 1$. The continuous overlap of the nanotube with the substrate—as opposed to the localized overlap of two nonparallel nanotubes—casts the problem in terms of the interaction energy per unit length, and the nanotube length L thus appears in Eq. (8).

Despite the complicated appearance, the physical foundations of the above formalism are not difficult to see. The vdW attraction arises from weighted spectral overlap in the anisotropic polarizability of the two bodies, and in spectrally complex dispersion media (such as water) this overlap can be screened by any relevant structure in the surrounding medium. Each mode n represents a "standing wave" of fluctuations between the two surfaces of interest. With the exception of the $n = 0$ term, each mode can thus have two orthogonal polarizations, which is why the $n = 0$ term is weighted by $1/2$. A physical discussion of these calculations and the significance of the various terms can be found in the book by Israelachvili.[1]

An empirical evaluation of the Hamaker coefficients is a straightforward numerical evaluation of the above expressions based on spectroscopic data. For the π plasmon, both the metallic and semiconducting nanotubes are characterized by two offset Lorentzians, one for each projection, with the anisotropy in the resonant energies and oscillator strengths fixed empirically from the isotropic features measured for each electronic type. Specifically, we use previous measurements of how the π plasmon in an unaligned film splits into two distinct features along and normal to the nanotube symmetry axis as the film is aligned.[30,40] Moving down in energy, the metallic ensemble has two axial resonant Lorentzian features and the semiconducting ensemble has three (Fig. 2), with no radial components. The low-energy ($E \to 0$) feature for each type is deduced from the Drude model of dielectric response applied to the measured resistivity of each film type.[26] The polymer substrate is modeled with 19 optically isotropic Lorentzian features.

The most dominant features are in the 10–20-eV range, which we are unable to directly measure for our materials. For the nanotubes, the $\sigma + \pi$ features are thus deduced from EELS of sparse mixed-type films extrapolated to zero momentum transfer.[35,36] We use the common π plasmon to bridge our measured optical spectra to the EELS spectra, with the f-sum rule and the measured ratio of mean diameters as a constraint. For the PDMS substrate, we use spectra based on low-loss EELS measured in the context of cryo-TEM and referenced to the well-known dielectric response function of amorphous ice.[45,46] Representative spectra are shown in Fig. 5. For the Lorentzian features, the relevant Kramers-Krönig transforms follow trivially by analogy with

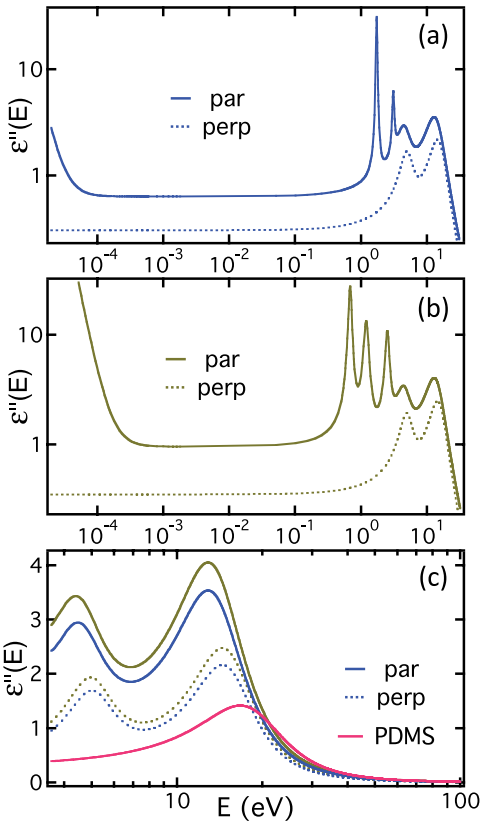

FIG. 5. (Color online) Anisotropic dielectric response for (a) the metallic SWCNTs and (b) the semiconducting SWCNTs over the full spectral window. (c) Detailed view of the two plasmons for each electronic type with the UV absorption used for the PDMS substrate.

the linear response of a damped harmonic oscillator. The angular overlap integrals in Eqs. (5), (6), and (9) are evaluated numerically for each Matsubara mode n, and the sums are then tabulated numerically (up to $n = 3000$) to compute the Hamaker coefficients for SWCNT-SWCNT interactions (semiconducting-semiconducting and metallic-metallic) and for SWCNT-PDMS interactions (metallic and semiconducting). Details are given in the supporting information.[39]

III. RESULTS AND DISCUSSION

A. Hamaker coefficients and pair potentials

For the SWCNT-SWCNT interaction, our analysis gives $A_0/k_BT = 46.5$ and $A_2/k_BT = 0.44$ for the semiconducting SWCNTs and $A_0/k_BT = 37.6$ and $A_2/k_BT = 0.26$ for the metallic SWCNTs. Figure 6(a) shows the full nanotube-nanotube interaction potential at a fixed relative orientation of 90° based on these coefficients, where we have introduced the repulsive Lennard-Jones term, $B(\ell/a)^{-7}$. The exponent of 7 reflects the same coarse-graining that transforms the usual ℓ^{-6} attraction into ℓ^{-1}, and we adjust B to achieve a minimum at $\ell/a = r/a - 2 = 0.33$ based on the interlayer spacing of graphite.[47,48] For the SWCNT-PDMS interaction, our analysis gives $A_0/k_BT = 33.4$ for the semiconducting SWCNTs and $A_0/k_BT = 30.1$ for the metallic SWCNTs. The total potential between the two nanotube types and the polymer substrate based on these Hamaker coefficients is shown in Fig. 6(b), where we assume a repulsive term of the form $B(\ell/a)^{-15/2}$ and adjust B to achieve a minimum at $\ell/a = 0.33$. In both cases, the semiconducting nanotubes have a significantly stronger attraction. The results are qualitatively consistent with the microscopic observations in Fig. 3, where the semiconducting SWCNTs show a greater tendency to bundle in marginally stable colloidal suspensions prepared under comparable conditions. For both electronic types, the suggested strength of the attraction to the PDMS substrate ($A_0 = 139$ zJ for the semis and $A_0 = 125$ zJ for the metals at 300 K) is surprising but not unprecedented. Recent experiments and simulations suggest that interactions between the methyl group of PDMS and the π-electron-rich surface of carbon nanotubes are favorable to carbon nanotube dispersion in PDMS, where the nanotubes are stabilized against aggregation by the adsorption of polymer chains.[49,50]

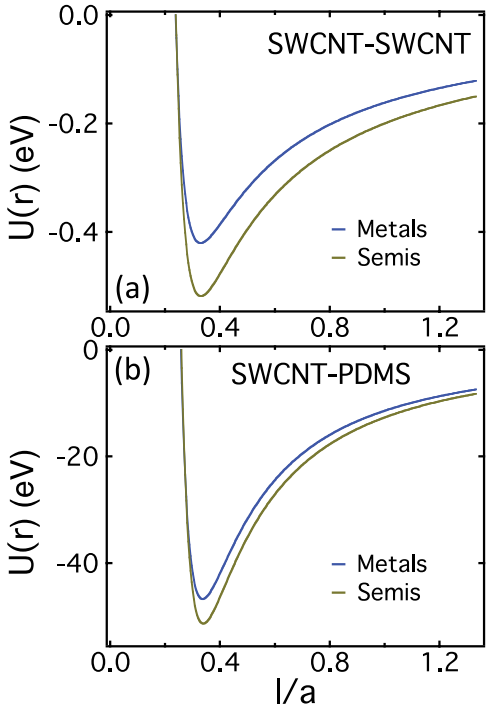

FIG. 6. (Color online) (a) Computed vdW potential between 90° crossed SWCNTs of each electronic type as a function of surface separation and (b) computed vdW potential between each type ($L/a = 250$) and the polymer (PDMS) substrate.

The Hamaker coefficients we compute here, $A_0 = 194$ zJ for semi-semi and $A_0 = 157$ zJ for metal-metal (300 K), are more than a factor of 2 larger than the near-field results computed in Ref. 27 for the (6,5) semiconducting and (9,3) metallic nanotubes. The major difference is the use of water as the intervening medium in Ref. 27 (as opposed to the use of air here), but there are significant differences in the absorption spectra of the nanotubes as well. The *ab initio* results in Ref. 27 give larger oscillator strengths, radial optical resonances, and greater spectral weight above 10 eV. Conversely, our results suffer from a lack of true spectral data above 5 eV, as we discuss in greater detail in the conclusion. We emphasize, however, that the trends are indeed similar, with both studies showing a modestly stronger attraction for semiconducting nanotubes.

For two isolated nanotubes crossed at an arbitrary angle θ, there is no stabilizing angular term in the full potential to prevent collapse into the global minimum at $\theta = 0$. Specifically, ignoring A_2 with respect to the much larger A_0, the potential for two isolated arbitrarily crossed SWCNTs ($\theta \neq 0$) is

$$\frac{U_{\rm tt}(r,\theta)}{k_BT} \simeq \frac{1}{\sin\theta}\left[\frac{B}{(\ell/a)^7} - \frac{A_0}{6(\ell/a)}\right], \qquad (10)$$

where "tt" denotes tube-tube and B is the repulsive LJ coefficient introduced above ($B = 1.45 \times 10^{-3}$ for the semis and $B = 1.15 \times 10^{-3}$ for the metals). This can be contrasted with results recently obtained from a "continuum" (pairwise) superposition of the atomic potentials, which has the form of an 8-2 expression.[51] The difference reflects our use of the near-field Lifshitz formalism, a point we consider again at the conclusion of the paper.

B. Scaling, electronic type, and film durability

The results presented here, taken as a whole, can explain a significant portion of the difference in the strain response of metallic versus semiconducting nanotube films.[26] Although the depth of the attractive well is 20–30 % deeper for the semis, both attractions are so much larger than k_BT that the nanotubes stick irreversibly on contact. Based on the measured size distributions, we can thus account for the observed difference in percolation threshold,[52] since $\phi_c \propto a/L$ gives $\phi_{cM}/\phi_{cS} \approx 2$, in excellent agreement with experiment.[26] This can have potentially significant manifestations, since for any critical quantity σ,

$$\sigma = \sigma_0(\phi/\phi_c - 1)^\alpha \simeq \sigma_0(\phi/\phi_c)^\alpha, \qquad (11)$$

well inside the percolation regime ($\phi \gg \phi_c$), and the ratio at comparable values of ϕ,

$$\sigma_S/\sigma_M \simeq (\sigma_{0S}/\sigma_{0M})(\phi_{cM}/\phi_{cS})^{\alpha}, \tag{12}$$

can thus become quite significant. The difference in attraction can further influence the strain response of the films because the depth and curvature of the interparticle potential can directly impact the modulus and yield strain of the network.[53] The role of SWCNT bending, buckling, and friction in network stability is a topic of considerable current interest.[54]

Specifically, we model the difference in attraction using scaling arguments borrowed from soft matter.[52–67] The SWCNTs have aspect ratios of 10^2–10^3 and Young moduli in the TPa range. Stretching and compression can thus be neglected, with bending being the only significant mode of deformation. The vdW attraction between nanotubes is strong and short-range in the absence of a surfactant and solvent, and the simplest description is through the contact energy per unit length, u, from which we get the energy for perpendicular contact,

$$w_p = 2ua', \tag{13}$$

where $a' \simeq a$ is the effective nanotube radius. Most theories of "sticky" fibers approximate the parallel potential by a simple square well of finite width, depth uL, and infinite height below a critical surface separation.[55] The network structure results from the interplay of bending, vdW attraction, excluded-volume interactions, static friction, and the initial conditions used to prepare the network.

For a random packing of long rods with excluded volume, entropy is irrelevant. The packing of such rods can be modeled by assuming independent and pairwise additive contacts.[56,57] This works for large-aspect-ratio rods (>15), colloidal rods, and macroscopic (>1 cm) fibers.[56] The orientational average of the excluded volume of a pair of randomly oriented rods gives the so-called "random-contact" equation of state,

$$\phi_c = \frac{c}{2}\frac{1}{\lambda}, \tag{14}$$

where $\lambda = L/2a$ is the aspect ratio and c is the average number of contacts per rod. Mechanical stability for random stacking implies $c = 10.8$, while $c \simeq 1$ for geometric percolation. In the latter case, Monte Carlo simulations of freely overlapping ellipsoids give $c = 1.502$ at $\lambda = 50$, with $c \to 1.2$ for $\lambda \geqslant 300$.[58] The theoretical result $c = 1$ applies to ideal (penetratable) rods, with simulations of ideal and hard rods confirming a slightly larger value, $c = 1.20$, for $\lambda \to \infty$.[52,59,65] For all these models, $\phi_c \propto 1/\lambda$ for long slender rods, both in and out of equilibrium and independent of spatial dimension.[61]

Equilibrium statistical mechanics predicts an exponential decrease in ϕ_c at moderate attraction.[63,64,66] For strong attraction ($w_p \simeq 20$–$40 k_B T$) and large aspect ratio ($\lambda \simeq 500$–1000), such theories predict unphysical values for ϕ_c, *many orders of magnitude* too small. This is not surprising, since the SWCNTs of interest are not in thermal equilibrium but form a glassy network. It is thus quite plausible to assume, as we did above, that the exact value of the attractive potential is not relevant to the onset of percolation; once the rods touch, they will permanently stick and rotate in response to the vdW torque (if not stabilized) before sliding into full parallel contact. There are three possible scenarios: (i) the formation of bundles of average size N; (ii) chain formation, where N aligned nanotubes overlap minimally at their ends; and (iii) the formation of a heterogeneous network of fractal aggregates.[57,62,66] In our system, all three effects presumably exist. Bundle formation reduces the aspect ratio to $\lambda' = \lambda/\sqrt{N}$ in Eq. (14), which causes ϕ_c to increase, while chain formation increases the effective aspect ratio to $\lambda' = N\lambda$. Nanotube deformation, in principle, leads to reduced λ', but this is assumed to be negligible near ϕ_c. For very long sticky rods, fractal aggregates are the dominant morphology, consistent with Fig. 1(c).

The 2D heterogeneous fiber network is a film of connected clusters of size R_C, as dictated by the method of deposition and surfactant removal. Each cluster is fractal, with $N \propto (R_C/l_C)^D$ and self-similarity between a lower cutoff l_C and R_C. A reasonable assumption is $l_C \simeq L$. A lower limit on R_C follows from the structure factor [Fig. 1(c)], with fractal scaling from $l_c \simeq 2.5\ \mu$m up to at least $2\pi/q_{\min} = 13\ \mu$m. Generalizing the theory from Ref. 55 to 2D gives

$$\phi_c = \frac{c}{2}\frac{1}{\lambda}\left(\frac{l_C}{R_C}\right)^{2\mathrm{D}}, \tag{15}$$

with $D = 1.72$ and $l_C/R_C = 1/13$. A larger range of self-similarity, $l_C/R_C = 100$, reduces ϕ_c by only a factor of 3.6. The scaling $\phi_c \simeq 1/\lambda$ is thus robust, with $\phi_c \approx 0.06\%$ for SWCNTs of length $L = 400$ nm. Fluctuations in film thickness, however, transform this volume fraction into a mean percolation thickness of several nanotube diameters.

Ignoring friction, the elastic properties of the film are dominated by the interplay between vdW forces, parametrized by u, and the bending rigidity, κ. These two quantities define the relevant length $L_W = \sqrt{\kappa/u} \sim$ 10–100 nm in dense networks well above percolation. The Young modulus has units of pressure, or energy per unit volume, with

$$E_0 \simeq \frac{uL_W}{L_W^3} \simeq \frac{u^2}{\kappa}. \tag{16}$$

With $u \sim A_0/a$, the ratio of the adhesion energies of two perpendicular fibers is

$$\left(\frac{w_{pS}}{w_{pM}}\right) = A_{0S}/A_{0M} \approx 1.25. \tag{17}$$

With $w_p = 2ua$ and $a_S/a_M = 0.85$, one finds

$$\frac{E_{0S}}{E_{0M}} = \left(\frac{a_M A_{0S}}{a_S A_{0M}}\right)^2 \approx 2.2 \tag{18}$$

as a prediction for the ratio of network modulus for each type. To explain the difference in yield strain, we invoke the scaling argument used to model fractal nanoparticle gels in the so-called "strong-link" regime, which models the film as a network of connected clusters. In this view, the yield strain is

$$\gamma_0 \propto E_0^{-(1+x)/(d+x)}, \tag{19}$$

where $d = 2$ is the spatial dimension and $x \approx 1$ is the "bond dimension."[67] We then obtain the ratio

$$\frac{\gamma_{0S}}{\gamma_{0M}} \approx \left(\frac{E_{0S}}{E_{0M}}\right)^{-2/3} \approx 0.6. \tag{20}$$

Details of the mechanical response will be reported elsewhere, but Eqs. (18) and (20) are in better than qualitative agreement with experiment.

IV. CONCLUSIONS

Using absorption spectra measured and inferred for type-purifed SWCNTs over a broad spectral window, we have empirically determined the magnitude of attractive nanotube-nanotube and nanotube-polymer potentials for each electronic type based on the Lifshitz theory of vdW-London dispersion interactions. Like a previous *ab initio* study,[27] our results suggest that semiconducting SWCNTs can have stronger vdW attraction, both to each other and to a cross-linked silicone elastomer (PDMS) substrate. The Hamaker coefficients we obtain for single SWCNT interactions in air are roughly a factor of 2 larger than those obtained from tight-binding *ab initio* studies in water.[27] This is because water, with its larger dielectric constant and absorption in the UV, will effectively "screen" correlations in the field terms [Eqs. (2) and (5)], thereby lowering the Hamaker constants.

Excitonic effects have a large influence on the optical properties of quasi-1D SWCNTs,[31] but in terms of the vdW-London dispersion spectra, the dominant features are the two plasmons. A combined optical/EELS study of aligned, type-sorted nanotube films would thus provide a more accurate foundation for what we have attempted here. For the semiconducting nanotubes, neglecting the three optical resonances reduces the Hamaker constant A_0 by roughly 5%, while neglecting the Drude term decreases the Hamaker constant by roughly 2%. For the metals, neglect of either of these terms reduces A_0 by roughly 3%. In this view, excitonic effects certainly have a measurable effect, but a larger question is how they influence the plasmons. From the *ab initio* perspective, a first-principles approach that correctly accounts for electron-hole interactions in quasi-1D systems would thus provide a more accurate computational foundation, but only to the extent that it also accurately describes the two plasmons. A higher-order computational scheme for the electronic band structure that invokes many-body Green functions would be required at the input level. Although this would clearly be a challenge, the significant computational advances of the recent past suggest that it might become feasible in the near future,[68–71] and we hope that the work we present here might help motivate such an effort. A deeper and more relevant question, however, is how the plasmonic features change—both in energy and oscillator strength—when a graphene sheet is rolled up into a tube.

A degree of care should be taken in terms of ascribing too much quantitative significance to our results, which are meant to substantiate trends and elucidate differences. Small variations in the London dispersion spectra can have large manifestations in the potential,[72] and we have not included any ionic effects,[73] nor have we addressed the nonpairwise additivity of vdW potentials in multilayered systems at large separations.[74] We have specifically limited our analysis to the near field to mitigate such effects. Similarly, our results can be contrasted with those obtained from a continuum superposition of the usual Lennard-Jones (LJ) 6-12 expression at the atomic level,[51] the so-called Girifalco potential.[75] A recent computation for 90° crossed SWCNTs based on such an approach gives a potential well of around 2 eV,[51] which is a factor of 4 stronger than what we find here. Uncertainty in the true oscillator strength of the 15 eV plasmon and the inherently macroscopic framework of the Lifshitz formalism might account for some of this discrepancy,[76] but a larger issue is the approximate nature of the continuum LJ approach.[27] The language of a "macroscopic" dielectric response function is in fact intrinsic to the correct many-body description of the optical SWCNT resonances,[31] while the continuum LJ approach obviously neglects any influence of the collective response implied by the optical resonances and plasmons.

Our results do, however, explain previously observed differences in the quiescent behavior and strain response of flexible SWCNT membranes based on electronic type.[26] Pristine nanotube networks are in some sense metastable with respect to deformation,[24] and the stronger attraction between semiconducting nanotubes, with the correspondingly lower percolation threshold, makes mechanical deformation in the semiconducting films more "plastic" than that in the metallic films, even at small strains and larger film thicknesses. To a large extent, however, this difference simply mirrors a difference in the mean diameter. Our observations thus shed significant light on important differences in the stability and durability of metallic and semiconducting nanotube networks that should help guide future modeling efforts, motivate new experiments, and better inform applications.

ACKNOWLEDGMENTS

E.K.H. and T.I. acknowledge the support of the National Science Foundation (NSF) through CMMI-0969155 and DMR-0706017. The authors thank Ji Yeon Huh and Jeffrey A. Fagan for supplying the type-purified nanotubes used in the study, and Steven D. Hudson for providing the TEM image in Fig. 1.

[1] J. N. Israelachvili, *Intermolecular and Surface Forces* (Elsevier, Waltham, MA, 2011).

[2] J. H. Seol, I. Jo, A. L. Moore, L. Lindsay, Z. H. Aitken, M. T. Pettes, X. Li, Z. Yao, R. Huang, D. Broido, N. Mingo, R. S. Ruoff, and L. Shi, Science **328**, 213 (2010).

[3] J. R. Royer, D. J. Evans, L. Oyarte, Q. Guo, E. Kapit, M. E. Mbius, S. R. Waitukaitis, and H. M. Jaeger, Nature (London) **459**, 1110 (2009).

[4] J. N. Munday, F. Capasso, and V. A. Parsegian, Nature (London) **57**, 170 (2009).

[5] B. W. Han, B. R. Herrin, M. D. Cooper, and I. A. Wilson, Science **321**, 1834 (2008).

[6] H. Nury, C. Van Renterghem, Y. Weng, A. Tran, M. Baaden, V. Dufresne, J. Changeux, J. M. Sonner, M. Delarue, and P. Corringer, Nature (London) **469**, 428 (2011).

[7] M. Xu, D. N. Futaba, T. Yamada, M. Yumura, and K. Hata, Science **330**, 1364 (2010).

[8] F. W. Delrio, M. P. De Boer, J. A. Knapp, E. D. Reedy, P. J. Clews, and M. L. Dunn, Nat. Mater. **4**, 629 (2005).

[9] A. Kis, G. Csanyi, J.-P. Salvetat, Thien-Nga Lee, E. Couteau, A. J. Kulik, W. Benoit, J. Brugger, and L. Forro, Nat. Mater. **3**, 153 (2004).

[10] Y. Lalatonne, J. Richardi, and M. P. Pileni, Nat. Mater. **3**, 121 (2004).

[11] G. A. Rance, D. H. Marsh, S. J. Bourne, T. J. Reade, and A. N. Khlobystov, ACS Nano **4**, 4920 (2010).

[12] H. B. G. Casimir, Proc. K. Ned. Akad. Wet. **51**, 793 (1948).

[13] E. M. Lifshitz, Sov. Phys. JETP **2**, 73 (1956).

[14] R. Saito, G. Dresselhaus, and M. S. Dresselhaus, *Physical Properties of Carbon Nanotubes* (Imperial College Press, London, 1999).

[15] R. H. Baughman, A. A. Zakhidov, and W. A. de Heer, Science **297**, 787 (2002).

[16] C. Wang, Q. Cao, T. Ozel, A. Gaur, J. A. Rogers, and M. Shim, J. Am. Chem. Soc. **127**, 11460 (2005).

[17] K. Yanagi, Y. Miyata, and H. Kataura, Appl. Phys. Express **1**, 034003 (2008).

[18] J. A. Fagan, M. L. Becker, J. Chun, and E. K. Hobbie, Adv. Mater. **20**, 1609 (2008).

[19] M. S. Arnold, J. Suntivich, S. I. Stupp, and M. C. Hersam, ACS Nano **2**, 2291 (2008).

[20] M. C. Hersam, Nature Nanotech. **3**, 387 (2008).

[21] X. Tu, S. Manohar, A. Jagota, and M. Zheng, Nature (London) **460**, 250 (2009).

[22] J. A. Fagan, M. L. Becker, J. Chun, P. Nie, B. J. Bauer, J. R. Simpson, A. Hight-Walker, and E. K. Hobbie, Langmuir **24**, 13880 (2008).

[23] Q. Cao and J. A. Rogers, Adv. Mater. **21**, 29 (2008).

[24] E. K. Hobbie, D. O. Simien, J. A. Fagan, J. Y. Huh, J. Y. Chung, S. D. Hudson, J. Obrzut, J. F. Douglas, and C. M. Stafford, Phys. Rev. Lett. **104**, 125505 (2010).

[25] J. M. Harris, G. R. S. Iyer, D. O. Simien, J. A. Fagan, J. Y. Huh, J. Y. Chung, S. D. Hudson, J. Obrzut, J. F. Douglas, C. M. Stafford, and E. K. Hobbie, J. Phys. Chem. C **115**, 3973 (2011).

[26] J. M. Harris, G. R. S. Iyer, A. K. Bernhardt, J. Y. Huh, S. D. Hudson, J. A. Fagan, and E. K. Hobbie, ACS Nano **6**, 881 (2012).

[27] R. F. Rajter, R. Podgornik, V. A. Parsegian, R. H. French, and W. Y. Ching, Phys. Rev. B **76**, 045417 (2007).

[28] R. H. French, J. Am. Ceram. Soc. **83**, 2117 (2000).

[29] V. A. Parsegian, *Van der Waals Forces* (Cambridge University Press, Cambridge, 2005).

[30] J. A. Fagan, J. R. Simpson, B. J. Landi, L. J. Richter, I. Mandelbaum, V. Bajpai, D. L. Ho, R. Raffaelle, A. R. Hight Walker, B. J. Bauer, and E. K. Hobbie, Phys. Rev. Lett. **98**, 147402 (2007).

[31] C. D. Spataru, S. Ismail-Beigi, L. X. Benedict, and S. G. Louie, Appl. Phys. A **78**, 1129 (2004).

[32] R. F. Rajter and R. H. French, Int. J. Mat. Res. **101**, 27 (2010).

[33] The f-sum rule relates the spectrum ϵ'' to the effective electron density of the material, $n_{\text{eff}} \propto \int_0^\infty \omega \epsilon''(\omega) d\omega$.

[34] T. Pichler, M. Knupfer, M. S. Golden, J. Fink, A. Rinzler, and R. E. Smalley, Phys. Rev. Lett. **80**, 4729 (1998).

[35] C. Kramberger, R. Hambach, C. Giorgetti, M. H. Rümmeli, M. Knupfer, J. Fink, B. Büchner, Lucia Reining, E. Einarsson, S. Maruyama, F. Sottile, K. Hannewald, V. Olevano, A. G. Marinopoulos, and T. Pichler, Phys. Rev. Lett. **100**, 196803 (2008).

[36] C. Kramberger, M. Rümmeli, M. Knupfer, J. Fink, B. Büchner, E. Einarsson, S. Maruyama, and T. Pichler, Phys. Status Solidi B **245**, 2284 (2008).

[37] O. Stéphan, D. Taverna, M. Kociak, K. Suenaga, L. Henrard, and C. Colliex, Phys. Rev. B **66**, 155422 (2002).

[38] A. G. Marinopoulos, L. Reining, and A. Rubio, Phys. Rev. B **78**, 235428 (2008).

[39] See Supplemental Material at http://link.aps.org/supplemental/10.1103/PhysRevB.85.245439 for details related to electronic type separation, film preparation/characterization, and determination of the full dielectric response.

[40] Y. Murakami, E. Einarsson, T. Edamura, and S. Maruyama, Phys. Rev. Lett. **94**, 087402 (2005).

[41] V. Perebeinos, J. Tersoff, and P. Avouris, Phys. Rev. Lett. **92**, 257402 (2004).

[42] J. A. Fagan, J.-Y. Huh, J. R. Simpson, J. L. Blackburn, J. M. Holt, B. A. Larsen, and A. R. Hight-Walker, ACS Nano **5**, 3943 (2011).

[43] B. J. Landi, H. J. Ruf, J. J. Worman, and R. P. Raffaelle, J. Phys. Chem. B **108**, 17089 (2004).

[44] E. K. Hobbie, J. Chem. Phys. **121**, 1029 (2004).

[45] S. Yakovlev and M. Libera, Micron **39**, 734 (2008).

[46] K. Kobayashi, J. Phys. Chem. **87**, 4317 (1983).

[47] B. I. Yakobson and L. S. Couchman, J. Nanopart. Res. **8**, 105 (2006).

[48] A. Carlson and T. Dumitrica, Nanotechnology **18**, 065706 (2007).

[49] A. Beigbeder, M. Linares, M. Devalkenaere, Ph. Degee, M. Claes, D. Beljonne, R. Lazzaroni, and P. Dubois, Adv. Mater. **20**, 1003 (2008).

[50] S. Marceau, P. Dubois, R. Fulchiron, and P. Cassagnau, Macromolecules **42**, 1433 (2009).

[51] A. I. Zhbanov, E. G. Pogorelov, and Y.-C. Chang, ACS Nano **4**, 5937 (2010).

[52] A. L. R. Bug, S. A. Safran, and I. Webman, Phys. Rev. Lett. **54**, 1412 (1985).

[53] A. R. Studart, E. Amstad, and L. J. Gauckler, Soft Matter **7**, 6408 (2011).

[54] A. N. Volkov and L. V. Zhigilei, ACS Nano **4**, 6187 (2011).

[55] P. van der Schoot and T. Odijk, J. Chem. Phys. **97**, 515 (1992).

[56] A. P. Philipse, Langmuir **12**, 1127 (1996).

[57] A. P. Philipse and A. M. Wierenga, Langmuir **14**, 49 (1998).

[58] E. J. Garboczi, K. A. Snyder, J. F. Douglas, and M. F. Thorpe, Phys. Rev. E **52**, 819 (1995).

[59] Z. Néda, R. Florian, and Y. Brechet, Phys. Rev. E **59**, 3717 (1999).

[60] M. Foygel, R. D. Morris, D. Anez, S. French, and V. L. Sobolev, Phys. Rev. B **71**, 104201 (2005).

[61] G. E. Pike and C. H. Seager, Phys. Rev. B **10**, 1421 (1974).

[62] G. M. H. Wilkins, P. T. Spicer, and M. J. Solomon, Langmuir **25**, 8951 (2009).

[63] B. Vigolo, C. Coulon, M. Maugey, C. Zakri, and P. Poulin, Science **309**, 920 (2005).

[64] R. Jadrich and K. S. Schweizer, J. Chem. Phys. **135**, 234902 (2011).

[65] M. Foygel, R. D. Morris, D. Anez, S. French, and V. L. Sobolev, Phys. Rev. B **71**, 104201 (2005).

[66] A. V. Kyrylyuk and P. van der Schoot, Proc. Natl. Acad. Sci. USA **17**, 8221 (2008).

[67] W.-H. Shih, W. Y. Shih, S.-I. Kim, J. Liu, and I. A. Aksay, Phys. Rev. A **42**, 4772 (1990).

[68]R. H. French, S. J. Glass, F. S. Ohuchi, Y. N. Xu, and W. Y. Ching, Phys. Rev. B **49**, 5133 (1994).
[69]W. Y. Ching, Y. N. Xu, and R. H. French, Phys. Rev. B **54**, 13546 (1996).
[70]Y. N. Xu, W. Y. Ching, and R. H. French, Phys. Rev. B **48**, 17695 (1993).
[71]Y. N. Xu and W. Y. Ching, Phys. Rev. B **51**, 17379 (1995).
[72]K. van Benthem, G. Tan, R. H. French, L. K. DeNoyer, R. Podgornik, and V. A. Parsegian, Phys. Rev. B **74**, 205110 (2006).
[73]R. Podgornik and V. A. Parsegian, Phys. Rev. Lett. **80**, 1560 (1998).
[74]R. Podgornik, R. H. French, and V. A. Parsegian, J. Chem. Phys. **96**, 858 (1992).
[75]L. A. Girifalco, J. Phys. Chem. **96**, 858 (1992).
[76]S. V. Rotkin and K. Hess, J. Comput. Electron. **1**, 323 (2002).